Preventing lithium ion battery failure during high temperatures by externally applied compression

Author: Yan Zhao[1], Yatish Patel[1], Ian A. Hunt[1], Kristina M. Kareh[2], Alexander A. Holland[1], Christian Korte[1], John P. Dear[1], Yan Yue[3, 4], Gregory J. Offer[1]

[1] Department of Mechanical Engineering, Imperial College London

[2] Department of Earth Science and Engineering, Imperial College London

[3] Beijing Institute of Aeronautical Materials (BIAM)

[4] Beijing Engineering Research Centre of Advanced Structural Transparencies for the Modern Traffic System

Keywords

Lithium-ion battery; High temperature; Compression; Degradation

Abstract

Lithium-ion cells can unintentionally be exposed to temperatures outside manufacturers recommended limits without triggering a full thermal runaway event. The question addressed in this paper is: Are these cells still safe to use? In this study, externally applied compression has been employed to prevent lithium ion battery failure during such events. Commercially available cells with Nickel Cobalt Manganese (NCM) cathodes were exposed to temperatures at 80ºC, 90ºC and 100ºC for 10 hours, and electrochemically characterised before and after heating. The electrode stack structures were also examined using x-ray computed tomography (CT), and post-mortems were conducted to examine the electrode stack structure and surface changes. The results show that compression reduces capacity loss by -0.07%, 4.95% and 13.10% respectively, measured immediately after the thermal testing. The uncompressed cells at 80ºC showed no swelling, whilst 90ºC and 100ºC showed significant swelling. The X-ray CT showed that the uncompressed cell at 100ºC suffered de-lamination at multiple locations after test, and precipitations were found on the electrode surface. The post-mortem results indicates the compressed cell at 100ºC was kept tightly packed, and the electrode surface was uniform. The conclusion is that externally applied compression reduces delamination due to gas generation during high temperature excursions.

1 Introduction

Lithium ion (Li-ion) batteries are increasingly favoured as the battery of choice for many sectors such as automotive, aerospace, consumer electronics and stationary storage. $LiMn_xNi_yO_2$ (NCM) cathodes are becoming increasing popular due to their high energy density. However, Li-ion batteries suffer from accelerated degradation at elevated temperatures [1–4] and thermal runaway in extreme cases [5,6].

The thermal runaway processes of the NCM chemistry are well described in the existing literature. From approximately 90ºC, the solid electrolyte interphase (SEI) starts to decompose exothermally [6–8]. This decomposition exposes the lithiated anode to the electrolyte which reacts with the lithiated anode to form a new SEI layer containing many impurities [9,10], and this is regarded as the initially dominant mechanism [5][11]. The SEI decomposition and reformation contribute to a reduction in electrolyte conductivity, the loss of lithium from the anode [12] and gas evolution. Prolonged exposure will also lead to electrolyte thermal decomposition. The decomposition of the $LiPF_6$ and carbonate electrolytes produces various impurities which lead to further capacity loss [13,14]. In addition some of the organic solvents in the electrolyte, such as EMC (ethyl methyl carbonate), have boiling points as low as 90ºC [15]. Thus, the evaporation could also cause significant gas generation. From 120ºC, the polymer separator starts to melt and localised short circuits can happen [16]. Internal short circuits will then generate heat internally and eventually lead to catastrophic cell failure as cathode decomposition occurs.

In recent years, most studies have focused on understanding the temperature driven degradation up to the manufacturer specified limit [3,17–20] or the onset/consequence of thermal runaway well above such limits [21–26]. Most cell manufacturers recommend cell operating and storage limits of around 50-60ºC [15]. However, in application, cells may be subjected to temperatures above the specified limits but below those necessary to trigger a full thermal runaway event. Feng et al characterised a set of large format NCM lithium ion cell

at temperatures between 80ºC and 160ºC [16]. The study concluded that the separator melting temperature was the limit for cell reusability. It was also found that cell capacity could be recovered by continuous cycling of the cell after the exposure. While the fading mechanisms were analysed using a mechanistic model, Feng et al did not provide an explanation for the cause of the capacity recovery behaviour.

Studies by Cannarella et al and Bonnick et al showed that a certain level of compressive stress could reduce capacity fade [27]. Cannarella et al theorised that the externally applied compression could prevent electrode stack de-lamination, thereby preventing the electrode surface became disconnected and reducing useable capacity. *Compression is often applied to lithium ion pouch cells during battery pack assembly to improve battery performance and mechanical stability*. Based upon the literature summarised above, degradation can be categorised into chemical or physical degradation. The chemical degradation is mostly a function of temperature and is caused by mechanisms including SEI layer decomposition and re-formation at the anode, electrolyte thermal decomposition, and loss of active material at the cathode. On the other hand, physical degradation is caused by delamination caused by gases produced by those chemical reactions and the evaporation of electrolyte species with a low boiling point, and is therefore both a function of temperature and the pressure, i.e. the mechanical boundary conditions of the cell layers such as degree of compression.

It is therefore expected that an externally applied compressive force could reduce the physical degradation by suppressing or preventing the delamination of layers. By applying compression to a pouch cell, the available volume for expansion could be restricted, which would increase the pressure and prevent the evaporation of electrolyte species with a low boiling point, and could perhaps even reduce the rate of reaction for those reactions which produce gases.

In order to test this hypothesis, we investigated the effect of external compression on cells exposed to high temperatures. A compressed and an uncompressed cell was used in the each of the high temperature tests. The cell was periodically characterised for a week after the high temperature test. X-ray Computed Tomography (CT) was employed to identify the cell internal

structure. The cells were also disassembled to examine the physical changes. We showed that degradation could be limited by externally applied compression,

2 Experimental

The 5Ah high power pouch cell used for this work is manufactured by Kokam (Model: SLPB11543140H5). The cell contains a graphite anode, $LiMnNiO_2$ (NCM) cathode. According to the specification sheet the electrolyte consists of a solution of $LiPF_6$ in a mixture of organic solvent Ethylene Carbonate (EC) and Ethymethyl Carbonate (EMC). The cell has a dimension of L 140 x W 42 x T 11.4 mm.

The environment temperature was controlled using a Binder KB53 incubator. Cell temperature was measured using K type thermocouples and recorded by using the TC-08 data logger from Pico technology.

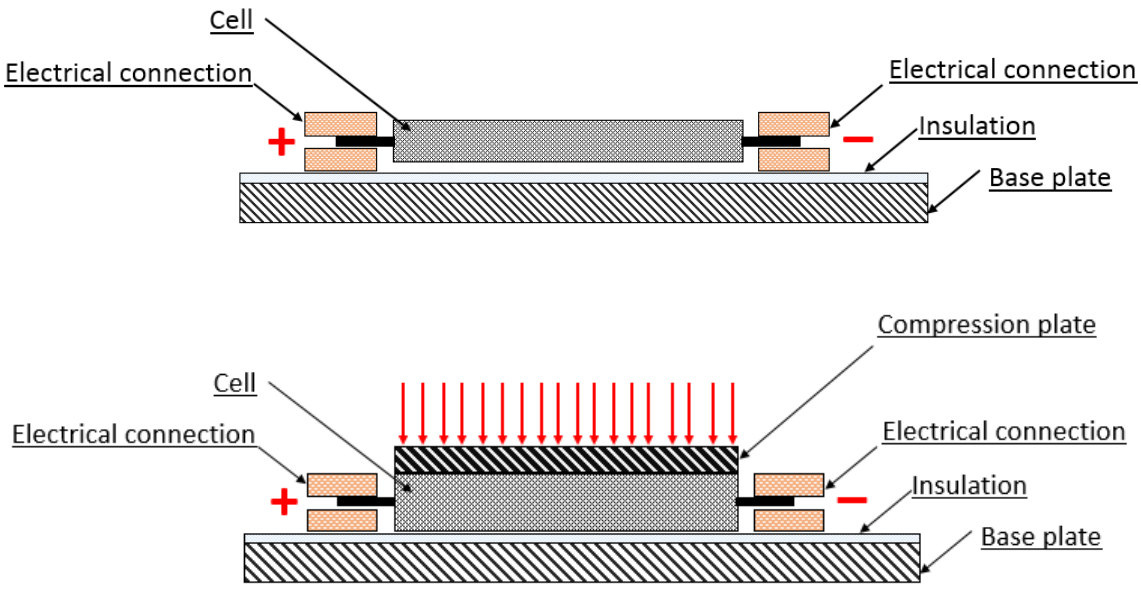


Figure 1. Cell connection setup: (a) uncompressed cell; (b) compressed cell.

For the compressed cells, a compressive force was applied on the L x W surface of the cell as shown in **Error! Reference source not found.**. The cell was loaded using the constant displacement method. To ensure a uniform load was applied, the compressive displacement

was set to 0.6 mm at all four corners of the cell. To ensure the loading is fully equalised, the cell was allowed to relax for 5 hr.

The fixed displacement was correlated to the load by performing a compressive loading and hold test. A fresh cell was tested on Instron (Model 3366). The fresh cell was compressed by 0.6 mm at a loading rate of 0.1 mm/min and was held there for 5 hrs. The load recorded at end of 5 hr period was taken as the load applied during the test.

Cells were characterised using a BioLogic BCS-815 battery cycler. The characterisation steps are shown in Table 1. The capacity was measured at discharge rates of 1C (5 A) and 3C (15A). The AC impedance was also measured at between 90% -10% state of charge (SoC) in steps of 10% where SoC was defined using the initial rated capacity of 5 Ah. The characterisation cycle was performed at 20 ºC in the incubator. Cells were allowed to thermally equalise to the temperature before each step.

2.1 X-ray imaging

Both a compressed and an uncompressed cell were imaged using a laboratory X-ray microtomography system (Phoenix v|tome|x, GE, USA) at 140 kV and 200 µA. 2400 images were captured on a detector of 4607 × 2304 pixels over one revolution of each cell, with an exposure time of 750 ms and a voxel size of 12.05 µm. A 0.1mm Cu filter was placed in front of the target to filter out low energy X-rays. The internal 3D structure of the cells was reconstructed using a filtered back-projection algorithm.

Table 1. Characterisation cycle at 20ºC.

Step	Description
1	Full depth 1C charge/discharge with constant voltage at 4.2V and 2.7V
2	Full depth 3C charge/discharge with constant voltage at 4.2V and 2.7V
3	Galvanostatic Electrochemical Impedance Spectroscopy (GEIS) from SOC 90% to 10% at 10% intervals, 10 mins rest period after each 1C pulse discharge.

2.2 Test sequence

To investigate the effect of the high temperature excursion on the cell performance, different cells were tested at 80ºC, 90ºC and 100ºC respectively. At each temperature, the cells were exposed to the high temperature for a period of 10 hr. To ensure uniformity, the fresh cells were characterised initially (D0). For the compressed cells the external compression was applied after the initial characterisation (D0). The external compression remained throughout subsequent tests. The compressed cells were then characterised again (D1) to examine the effect of applying the compression. To ensure a comparable cycling history, the uncompressed cell applied was also characterised again (D1).

Subsequently, both cells were subjected to a 10hr exposure to the high temperature environment. The cells were characterised again after heating (D2). Finally, cells were periodically (every 24 hr.) characterised for approximately one week (D3-D6). All the characterisations were conducted as described in Table 1.

Table 2. Test sequence description.

Sequence number	Description
D0	Initial characterisation
D1	Characterisation immediately after external load applied
D2	Characterisation after high temperature excursion
D3	Periodic characterisation 1
D4	Periodic characterisation 2
D5	Periodic characterisation 3
D6	Periodic characterisation 4

3 Results and discussion

3.1 Effect of compression

The compressive load was measured at the displacement of 0.6 mm with the loading rate of 0.1mm/min after 5hr relaxation. The load was found to be 1447 N which is equivalent to an approximate pressure of 0.32 MPa on the cell surface.

The cell was characterised before (D0) and after the compression (D1). As detailed in Table 3, the cell capacities dropped by approximately 0.4%. As shown in Figure 2b, the discharge curve and ICA curve were similar before and after the compression. The Incremental Capacity Analysis (ICA) peak at 3.7V reduced by 0.04 Ah/V, and he EIS spectras shifted in a more positive direction along the real axis by approximately 0.15 mΩ i.e. the polarisation resistance increased, as shown in Figure 3. Overall, the cell performance was very similar before and after compression was applied.

Table 3. The capacity of the cells measured at 1C before (D0) and after the compression was applied (D1): cell 1 for 80 ºC test, cell 2 for 90ºC test and cell 3 for 100ºC test.

	Capacity change before and after compression [mAh]		
	Cell 1	Cell 2	Cell 3
Before (D0)	4915	4980	4935
After (D1)	4892	4958	4917
Loss	-0.47%	-0.44%	-0.36%

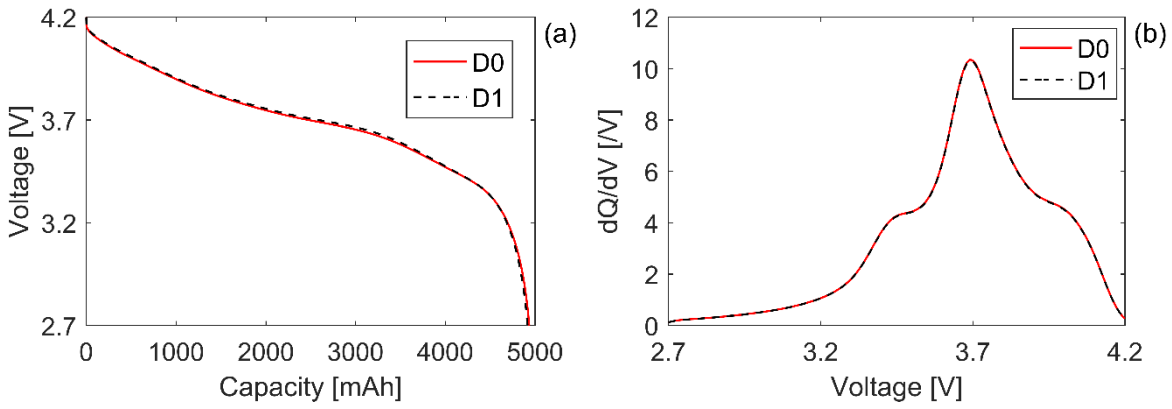


Figure 2. Comparison before (D0) and after (D1) (a) 1C discharge curve, (b) incremental capacity analysis curve.

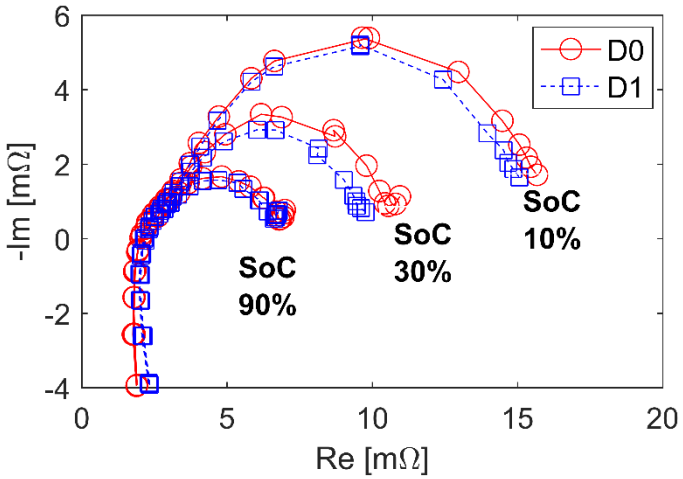


Figure 3. EIS measurements before (D0) and after (D1) compression, the measurement taken at SoC 90%, 30% and 10%.

3.2 Capacity measurements

It was shown that the compression causes approximately 0.4% reduction in capacity. Figure 4 shows the normalised capacities from the initial characterisation (D0) to post high temperature characterisation (D6). To better understand the degradation, the data will be analysed in two different regions: (i) the immediate damage (i.e. change from after compression (D1) to immediately after heating (D2)) and (ii) the longer term effect (i.e. D2 to D6). For the uncompressed cells tested at 90ºC, the final characterisation data at D6 is missing due to faulty equipment. D5 is the characterisation done 24 hours prior to the D6. Therefore, the comparison between capacity measurements will only be made up to D5.

Table 4 shows the detailed capacity change from before (D1) and immediately after high temperature exposure (D2). For the uncompressed cell tested at 100ºC, the capacity dropped by 13.1% compared to the compressed cell. For the uncompressed cell tested at 90ºC, the capacity dropped by 4.95% compared to the compressed cell. Both cells tested at 80ºC performed similarly.

Table 4. The capacity of the cells measured at 1C before (D1) and immediately after the high temperature exposure (D2): cell 1 for 80 ºC test, cell 2 for 90ºC test and cell 3 for 100ºC test.

	Capacity change-before(D1) and after(D2) heating

	Cell 1 -80ºC	Cell 2 -90ºC	Cell 3 -100ºC
Compressed	-1.21%	-2.29%	-4.12%
Uncompressed	-1.14%	-7.24%	-17.22%
Difference	-0.07%	+ 4.95%	+ 13.10%

Table 5 shows the capacity change from measurement point D2 (immediately after high temperature test) to D5 (approximately 5 days after the high temperature test). Compressed cells did not show any capacity recovery from D2 to D5. For the uncompressed cells tested at 100ºC and 90ºC, the capacity recovered by 6.65% and 3.25% respectively. For the uncompressed cell tested at 80ºC, the capacity remained constant from D2 to D5.

Significant cell swelling was observed for uncompressed cells during testing at 100ºC and 90ºC, while there was no visible swelling observed at 80ºC. The swelling disappeared almost immediately when the cell was cooled. For cell tested at 100ºC and 90ºC, wrinkles were observed on the pouch surface after cooling down. Therefore, it was assumed the cell swelling was mainly caused by the evaporation of the electrolyte, as it is highly unlikely gases produced by side reactions will suddenly disappear upon cooling. We therefore concluded that the primary mechanism by which compression reduces degradation at temperatures above 80ºC is by increasing the pressure and suppressing electrolyte evaporation.

Table 5. The capacity of the cells measured at 1C after the high temperature exposure (D2) and after prolonged resting (D5): cells tested at 80 ºC, cells tested at 90ºC and cells tested at 100ºC test.

	Capacity change – post the high temperature test (D2) and after prolonged resting (D5)		
	Cell 1 -80ºC	Cell 2 -90ºC	Cell 3 -100ºC
Compressed	+0.68%	-0.25%	-0.23%
Uncompressed	-0.30%	+3.00%	+6.42%
Difference	+0.98%	-3.25%	- 6.65%

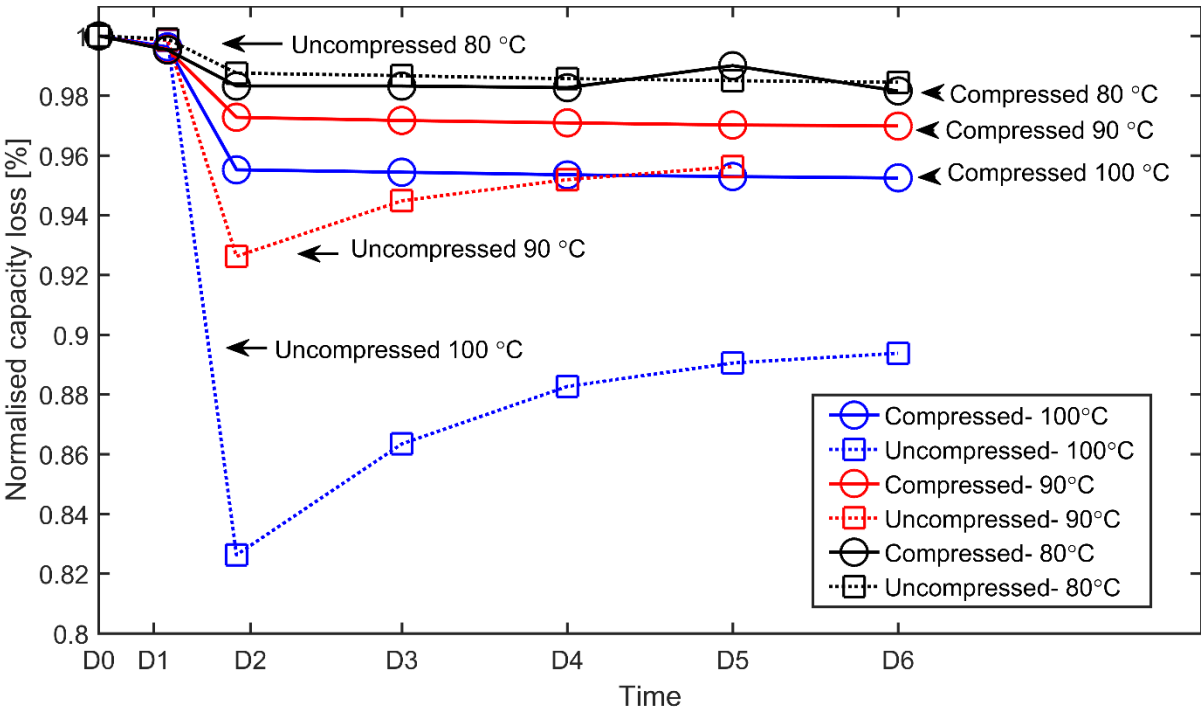


Figure 4. Capacity measurements at 1C discharge from immediately after heating (D1) to after prolonged resting (D6), compressed cells and uncompressed tested at 80ºC, 90ºC and 100ºC

For uncompressed cells tested at 100ºC and 90ºC, the capacity measured from D1 to D5 showed two distinct regions, where the capacity dropped sharply after D1 followed by a gradual increase from D2 to D5. Thus, it is important to examine the discharge curves in order to understand the differences. The effect was the most pronounced for cells tested at 100ºC.

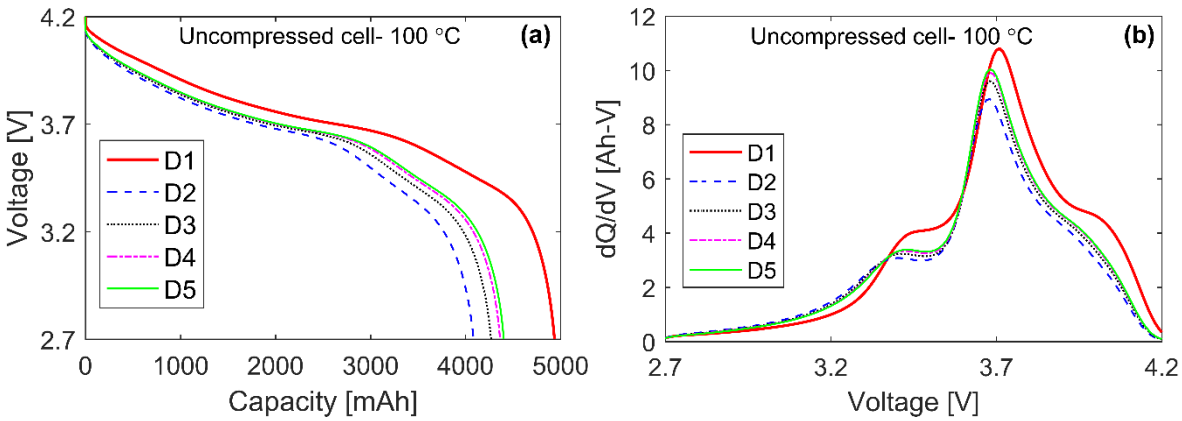
Figure 5 shows the discharge curve and the corresponding incremental capacity analysis (ICA) curves for the cells tested at 100ºC. Probability density function method was used to obtain the ICA curves [28]. For the uncompressed cell immediately after heating, the plateau/peak at 3.71V and 3.45V shifted to 3.68V and 3.41V respectively. The peak intensity was also reduced from 10.8 Ah/V at 3.71V to 8.94 Ah/V at 3.68V, which indicates an increase in cell impedance. From D2 to D5, the peak intensity recovered to 10.05 Ah/V without a shift in the peak position. This indicates a decrease in cell impedance. The lowering of the peaks across the entire voltage range indicates this was due to an Ohmic resistance increase.

Figure 5c and Figure 5d show the same discharge curve and the ICA curves for the compressed cell. There was no shift in the plateau/peak at 3.70V from D1 to D2. The peak

intensity also remained similar, 10.64 Ah/V and 10.97 Ah/V respectively. However, the peak intensity around 3.4V dropped from approximately 4.176 Ah/V to 3.44 Ah/V, which shows the cell impedance may have increased slightly at lower SoC.

From D1 to D2, compression appears to increase the cell impedance at lower SoC as the voltage curve is only lower towards the end of discharge. It results in a significant reduction in the capacity as the lower voltage cut-off would be reached sooner. For the compressed cell and the uncompressed cell, the ICA curves change towards end of discharge showed similarity in terms of the change in peak intensity and position. The similarity could be attributed to a similar interfacial resistance change at the anode as the result of the high temperature exposure as the charge transfer resistance of the anode is only likely to become rate limiting at low SoC.

From D2 to D5, the compression eliminated the capacity recovery process for cells tested at 100^{o} C and 90^{o} C. For uncompressed cells, the capacity and impedance continue to evolve sometime after the cooling. Therefore, it is important to examine AC impedance results to further understand the difference the compression introduces to the degradation process.



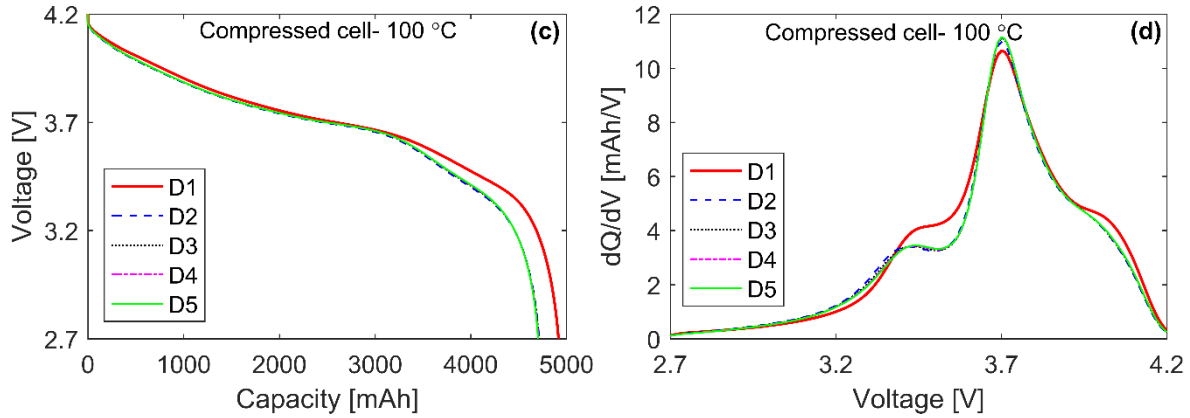


Figure 5. Plots for cells tested at 100ºC, characterised from D1 to D5: (a) Uncompressed cell 1C discharge curve, (b) Uncompressed cell ICA curves, (c) Compressed cell 1C discharge curve, (d) Compressed cell ICA curves.

3.3 ElS measurements

EIS was conducted as part of each characterisation cycle. Figure 6a, shows the spectra for the uncompressed cell tested at 100º C measured at 50% SoC from D1 to D5. Between D1 and D2, the spectra shifted significantly towards the right. The intersection with real axis is interpreted as the ohmic resistance of the cell. As measurement was done on complete cells, it was hard to associate the lower frequency resistances to exact internal processes. Therefore, the magnitude of associated polarisation resistance are only examined comparatively. From D2 to D5, the low frequency impedance decreased gradually, while the high frequency impedance stayed relatively constant. The decrease in the diameters was attributed to a decrease in polarisation resistance. For the compressed cell tested at 100º C, the high frequency impedance increased but the low frequency impedance did not increase significantly after heating as shown in Figure 6b. The EIS results were fitted using ZVIEW fitting software from Scribner Associates using the model shown in Figure 6c. The fitting results are shown in the Figure 6d and Figure 6e.

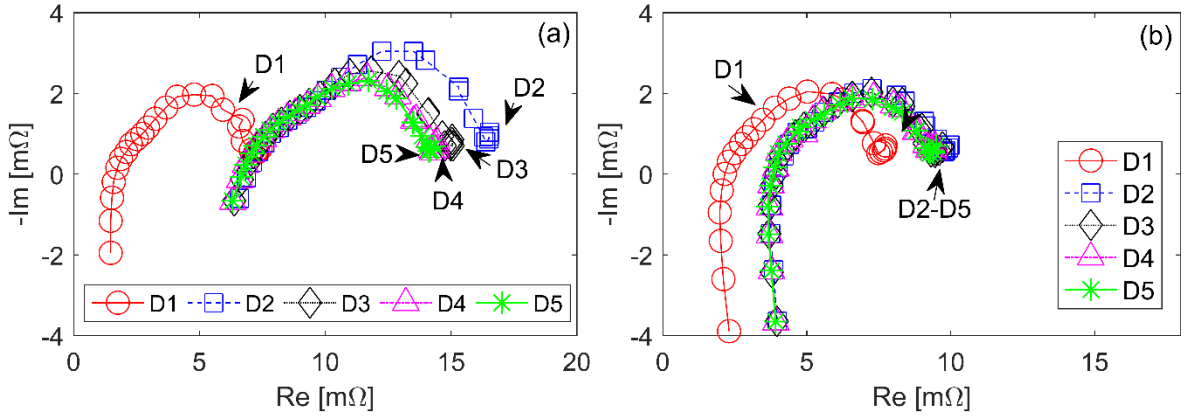
From D1 to D2, for the uncompressed cell, the series resistance R_s increased from 1.378 mΩ to 5.415 mΩ as shown in Figure 6d. The series resistance of the compressed cell increased

from 1.963 mΩ to 3.724 mΩ. The low frequency polarisation resistance R_2 increased significantly for uncompressed cell, from 1.13 mΩ to 8.16 mΩ. In comparison, R_2 for the compressed cell increased slightly from 0.79 mΩ to 0.94 mΩ.

From D2 to D5, R_s was stable for both cells. For the compressed cell, R_1 continued to decrease, from 8.15 mΩ at D2 to 6.73 mΩ at D5. This reduction correlates well with the continued capacity recovery shown in Figure 5.

The fitting results correlate well with the capacity measurements and general discharge curve shape change descried in in section 3.4. EIS result confirmed that the resistance changes were driving the capacity evolution. The initial rise in series resistance and polarisation resistance was induced by heating. The subsequent capacity recovering was the result of the reduction in polarisation resistance.

From this analysis it was concluded that the high temperature excursion caused irreversible chemical degradation, which gave rise to the changes between D1 and D2. Compressed cells showed no further degradation and the performance was stable after cooling. For uncompressed cells, the performance slowly increased, and based upon the previous conclusion that significant electrolyte evaporation occurred for cells tested at 90° C and 100° C the hypothesis that layers and/or regions of layers dried out during electrolyte evaporation, and during the rest and characterisation period the condensed electrolyte slowly re-wets the electrodes of those layers that were dried out.



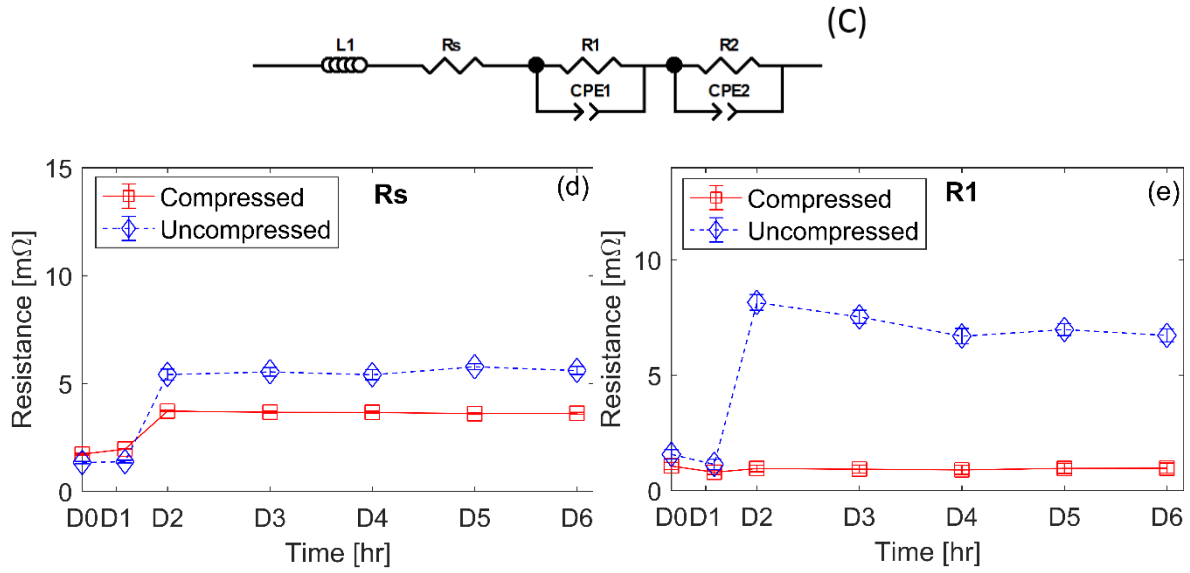


Figure 6 EIS fitting results R_s is the series resistance, R_1 is the low frequency polarisation resistance

3.4 X-ray computed tomography image

As discussed, it was hypothesised that compression would increase the pressure within a cell and prevent evaporation and by mechanically holding the laminated cell stack together would prevent any potential delamination caused by gas generation. Hence, X-ray CT imaging was used to examine the two cells after testing at 100^{o} C.

Figure 7 shows the cross sectional CT image data for both cells. For the compressed cell, the electrode stack is shown to be very uniform. It is hard to distinguish between the individual layers. For the uncompressed cell, the electrode layers were more clearly defined in the image. Suggesting a more loosely packed cell. There were signs at a few locations (marked with red arrows) of localised separation between electrodes and separators.The delamination could lead to the loss of the active reaction area, thereby increasing cell impedance and reaction in capacity. Due to both the size of the sample and the image resolution, it was hard to conduct a quantitative analysis of the size of the delamination. However, the qualitative comparison of both cells correlates well with the capacity and impedance measurements.

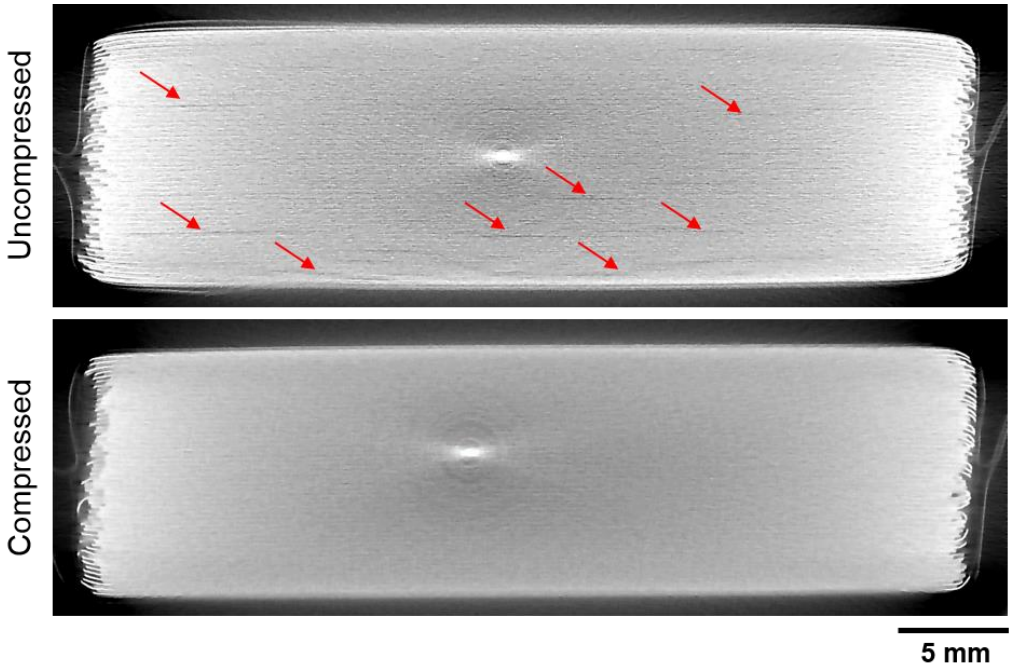


Figure 7 CT image of the compressed and uncompressed cell after the test at 100ºC

3.5 Cell disassembly

To further investigate the cell electrode stack structural and surface changes, both cells tested at 100^{o} C were disassembled as shown in Figure 8. For the uncompressed cell, the electrode stack was not tightly packed upon opening, and a brown coloured precipitate was observed on both anodes and cathodes.

For the compressed cell, there was excess discoloured electrolyte present at the edge of the pouch, and the outside layer of the separator wrap was discoloured. The discoloration reduced as the separator was unwrapped toward the inner layers. The cell stack was tightly packed and layers were in full surface contact. The removed electrode layers were show a uniform black colour without any precipitates. The excess electrolyte found in the pouch could be caused by the mechanical compression, where the electrolyte was pushed out from the electrodes due to reduction in the stack volume. The electrolyte reduction in the cell stack could lead to reduction in the electrical conductivity, therefore increasing the ohmic resistance. This observation therefore correlates well with the cell capacity reduction from D0 to D1 discussed in section 3.1. Based on the observation made by Sloop et al, it was thought that

the brown solution and precipitation was the product of the thermally decomposed electrolyte[29]. For the uncompressed cell, the decomposed solution was able to renter the electrode stack as there was no physical constraint. The electrolyte and decomposition products were then able to gradually rewet the electrode layers. For the compressed cell, it was thought that the displaced electrolyte was not able to rewet electrode stack due to the compressed stack, therefore the brown solution was present only in the pouch and separator wrap.

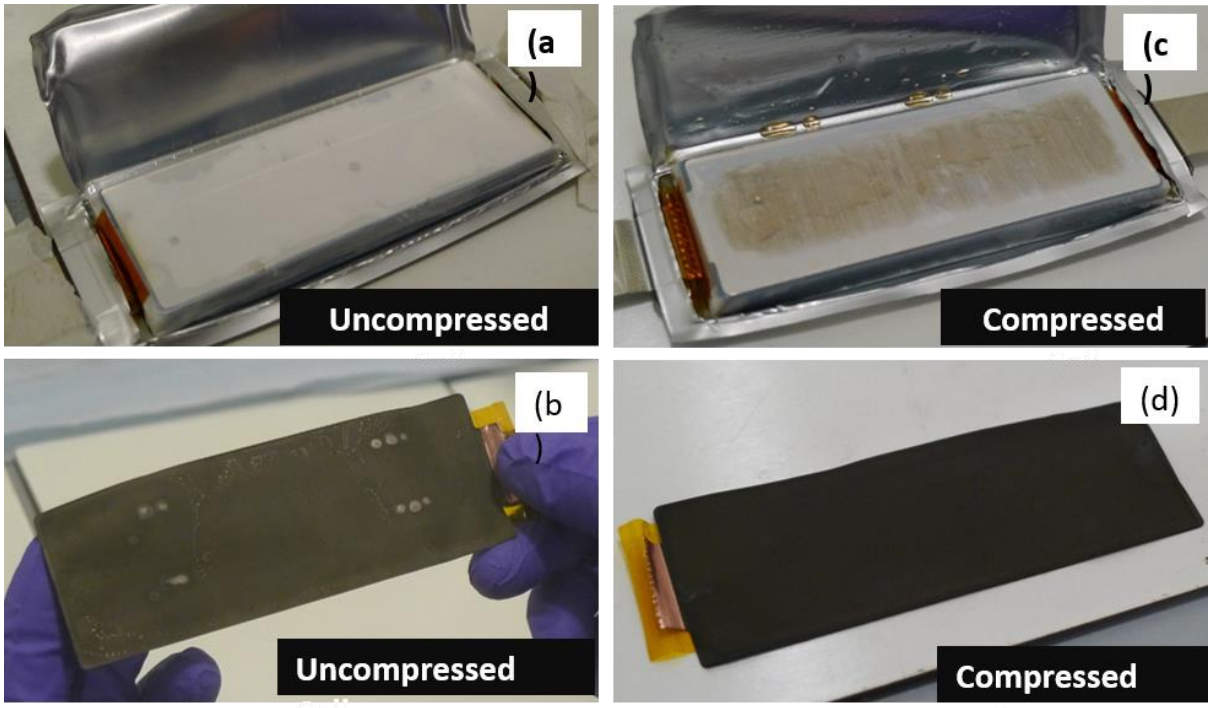


Figure 8 Image of the electrode after high temperature test

4 Conclusion

Lithium ion pouch cells with Nickel Cobalt Manganese (NCM) cathodes were exposed to temperatures of 80^{o} C, 90^{o}C and 100^{o}C for 10 hours. One set of cells was compressed and

the other was not. Cells were periodically characterised after the high temperature test and X-ray CT was used to probe the structural change in the electrodes stack. Cells were also disassembled to examine the physical change due to the heating and the compression.

For cells tested at 100ºC and 90ºC, it was shown that the degradation could be reduced by applying external compression. Compression improved the capacity loss measured immediately after cooling by 13.10% and 4.95% respectively. The cells tested at 80ºC saw no significant difference between compression or not. Further characterisation showed an improvement over time in the capacity of the cells which were uncompressed. However the capacity did not recover to the same level as the cells that were compressed. Cells which were compressed showed no change in capacity over time. Electrochemical impedance spectroscopy indicated that the uncompressed cells suffered significant increases in both low and high frequency impedance, compared to the compressed cells. The x-ray CT images and cell post-mortem revealed that the applied compression prevented the localised de-lamination inside the electrodes stack.

The results showed that compression does not appear to have any impact on the rate of chemical degradation. However, compression does have a significant impact on the consequences of that degradation on mechanical changes to the cell at temperatures above 80ºC, by increasing the pressure inside the cell and preventing layers from delaminating. The compression, by increasing the pressure, also prevented significant electrolyte evaporation from occurring and again preventing layers from delaminating. The recovery in capacity after the high temperature excursion for cells that were not compressed was interpreted as electrolyte condensing and slowing rewetting the electrode layers. The benefit of the compression will diminish when other degradation mechanisms including separator melting and subsequent localised internal short circuit become dominant.

Acknowledgement

Much appreciated is the strong support received from Beijing Institute of Aeronautical Materials (BIAM). The research was performed at BIAM-Imperial Centre for Materials Characterisation, Processing and Modelling at Imperial College London

Reference.

[1] P. Ramadass, B. Haran, R. White, B.N. Popov, Capacity fade of Sony 18650 cells cycled at elevated temperatures: Part I. Cycling performence, J. Power Sources. 112 (2002) 614–620. doi:10.1016/S0378-7753(02)00473-1.

[2] K. Jalkanen, J. Karppinen, L. Skogström, T. Laurila, M. Nisula, K. Vuorilehto, Cycle aging of commercial NMC/graphite pouch cells at different temperatures, Appl. Energy. 154 (2015) 160–172. doi:10.1016/j.apenergy.2015.04.110.

[3] T. Waldmann, M. Wilka, M. Kasper, M. Fleischhammer, M. Wohlfahrt-Mehrens, Temperature dependent ageing mechanisms in Lithium-ion batteries - A Post-Mortem study, J. Power Sources. 262 (2014) 129–135. doi:10.1016/j.jpowsour.2014.03.112.

[4] J. Vetter, P. Novák, M.R. Wagner, C. Veit, K.C. Möller, J.O. Besenhard, M. Winter, M. Wohlfahrt-Mehrens, C. Vogler, a. Hammouche, Ageing mechanisms in lithium-ion batteries, J. Power Sources. 147 (2005) 269–281. doi:10.1016/j.jpowsour.2005.01.006.

[5] A.S. Gozdz, J.M. Thrascon, S. Gebizlioglu, A. Du Pasquier, F. Disma, S.A.S. Gozdz, J.M. Tarascon, Differential Scanning Calorimetry Study of the Reactivity of Carbon Anodes in Plastic Li-Ion Batteries, 145 (1998) 472–477.

[6] N. Tanaka, W.G. Bessler, Numerical investigation of kinetic mechanism for runaway thermo-electrochemistry in lithium-ion cells, Solid State Ionics. 262 (2014) 70–73. doi:10.1016/j.ssi.2013.10.009.

[7] M.N. Richard, Accelerating Rate Calorimetry Study on the Thermal Stability of Lithium Intercalated Graphite in Electrolyte. I. Experimental, J. Electrochem. Soc. 146 (1999) 2068. doi:10.1149/1.1391893.

[8] H. Maleki, Thermal Stability Studies of Li-Ion Cells and Components, J. Electrochem. Soc. 146 (1999) 3224. doi:10.1149/1.1392458.

[9] M.N. Richard, Accelerating Rate Calorimetry Study on the Thermal Stability of Lithium Intercalated Graphite in Electrolyte. II. Modeling the Results and Predicting Differential Scanning Calorimeter Curves, J. Electrochem. Soc. 146 (1999) 2078. doi:10.1149/1.1391894.

[10] G.G. Botte, R.E. White, Z. Zhang, Thermal stability of LiPF6–EC:EMC electrolyte for lithium ion batteries, J. Power Sources. 97–98 (2001) 570–575. doi:10.1016/S0378-7753(01)00746-7.

[11] U. Vonsacken, E. Nodwell, A. Sundher, J.R. Dahn, Comparative Thermal-Stability of Carbon Intercalation Anodes and Lithium Metal Anodes for Rechargeable Lithium Batteries, Solid State Ionics. 69 (1994) 284–290. doi:10.1016/0167-2738(94)90417-0.

[12] P. Arora, R.E. White, M. Doyle, Capacity fade mechanisms and side reactions in lithium-ion batteries, J. Electrochem. Soc. 145 (1998) 3647–3667.

http://www.scopus.com/inward/record.url?eid=2-s2.0-0032188340&partnerID=tZOtx3y1.

[13] B. Ravdel, K.M. Abraham, R. Gitzendanner, J. DiCarlo, B. Lucht, C. Campion, Thermal stability of lithium-ion battery electrolytes, J. Power Sources. 119–121 (2003) 805–810. doi:10.1016/S0378-7753(03)00257-X.

[14] C.L. Campion, W. Li, B.L. Lucht, Thermal Decomposition of LiPF[sub 6]-Based Electrolytes for Lithium-Ion Batteries, J. Electrochem. Soc. 152 (2005) A2327. doi:10.1149/1.2083267.

[15] PSE, Kokam superior Lithium Polymer Material Safety Data sheet Batteries, (2011) 1–12.

[16] X. Feng, J. Sun, M. Ouyang, X. He, L. Lu, X. Han, M. Fang, H. Peng, Characterization of large format lithium ion battery exposed to extremely high temperature, J. Power Sources. 272 (2014) 457–467. doi:10.1016/j.jpowsour.2014.08.094.

[17] H.F. Jin, Z. Liu, Y.M. Teng, J.K. Gao, Y. Zhao, A comparison study of capacity degradation mechanism of LiFePO4-based lithium ion cells, J. Power Sources. 189 (2009) 445–448. doi:10.1016/j.jpowsour.2008.12.124.

[18] Y. Zhang, C.Y. Wang, X. Tang, Cycling degradation of an automotive LiFePO4 lithium-ion battery, J. Power Sources. 196 (2011) 1513–1520. doi:10.1016/j.jpowsour.2010.08.070.

[19] B. Wu, V. Yu, Y. Merla, R.F. Martinez-botas, N.P. Brandon, G.J. Offer, Differential thermal voltammetry for tracking of degradation in lithium-ion batteries, 273 (2015) 495–501. doi:10.1016/j.jpowsour.2014.09.127.

[20] M. Dubarry, B.Y. Liaw, M.-S. Chen, S.-S. Chyan, K.-C. Han, W.-T. Sie, S.-H. Wu, Identifying battery aging mechanisms in large format Li ion cells, J. Power Sources. 196 (2011) 3420–3425. doi:10.1016/j.jpowsour.2010.07.029.

[21] R. Saada, D. Patel, B. Saha, Causes and consequences of thermal runaway incidents - Will they ever be avoided?, Process Saf. Environ. Prot. 97 (2015) 109–115. doi:10.1016/j.psep.2015.02.005.

[22] P.T. Coman, S. Rayman, R.E. White, A lumped model of venting during thermal runaway in a cylindrical Lithium Cobalt Oxide lithium-ion cell, J. Power Sources. 307 (2016) 56–62. doi:10.1016/j.jpowsour.2015.12.088.

[23] A. Melcher, C. Ziebert, M. Rohde, H.J. Seifert, Modeling and simulation of the thermal runaway behavior of cylindrical Li-ion cells-computing of critical parameters, Energies. 9 (2016) 1–19. doi:10.3390/en9040292.

[24] X. Feng, M. Fang, X. He, M. Ouyang, L. Lu, H. Wang, M. Zhang, Thermal runaway features of large format prismatic lithium ion battery using extended volume accelerating rate calorimetry, J. Power Sources. 255 (2014) 294–301. doi:10.1016/j.jpowsour.2014.01.005.

[25] A.W. Golubkov, D. Fuchs, J. Wagner, H. Wiltsche, C. Stangl, G. Fauler, G. Voitic, A. Thaler, V. Hacker, Thermal-runaway experiments on consumer Li-ion batteries with metal-oxide and olivin-type cathodes, RSC Adv. 4 (2014) 3633–3642. doi:10.1039/C3RA45748F.

[26] Q. Wang, P. Ping, X. Zhao, G. Chu, J. Sun, C. Chen, Thermal runaway caused fire and explosion of lithium ion battery, J. Power Sources. 208 (2012) 210–224. doi:10.1016/j.jpowsour.2012.02.038.

[27] S.F. Schuster, T. Bach, E. Fleder, J. Müller, M. Brand, G. Sextl, A. Jossen, Nonlinear aging characteristics of lithium-ion cells under different operational conditions, J. Energy Storage. 1 (2015) 44–53. doi:10.1016/j.est.2015.05.003.

[28] X. Feng, J. Li, M. Ouyang, L. Lu, J. Li, X. He, Using probability density function to evaluate the state of health of lithium-ion batteries, J. Power Sources. 232 (2013) 209–218. doi:10.1016/j.jpowsour.2013.01.018.

[29] S.E. Sloop, J.K. Pugh, S. Wang, J.B. Kerr, K. Kinoshita, Chemical Reactivity of PF[sub 5] and LiPF[sub 6] in Ethylene Carbonate/Dimethyl Carbonate Solutions, Electrochem. Solid-State Lett. 4 (2001) A42. doi:10.1149/1.1353158.